Controlled chloride cracking of austenitic stainless steel tube samples

by M.S. Raseroka* and P.C. Pistorius†

Synopsis

An experimental rig has been constructed to produce chloride stress corrosion cracks in Type 304L stainless steel tube samples. The samples are to be used to test possible *in situ* repair methods in future work. The factor which influences the time to failure most strongly is the sample temperature; the distribution of cracks within the sample is affected by local temperature variations and by the position of the water line. Low-frequency oscillations in stress, caused by the on-off temperature controller, did not appear to influence cracking in these tests.

Introduction

Austenitic stainless stainless steels can undergo stress corrosion cracking in chloride-containing environments; such 'chloride cracking' generally occurs at temperatures above 60ºC.[1,2], The macroscopic path of the cracks is mainly perpendicular to the applied load or stress.

When stainless steel components exhibit stress corrosion cracking in service plant operators can replace or repair the components. In some instances it may be cost-effective to repair a stress corrosion cracked component *in situ*. A combination of high replacement costs, scarcity of material and/or long lead times in procuring new material, may render component repair a viable option. Tungsten inert gas arc welding and recently, laser and friction welding have been researched as repair methods for stress corrosion cracked components[3,4]. This study forms part of a bigger project undertaken to evaluate the feasibility of doing an *in situ* weld repair on a leaking stress corrosion cracked component, of Type 304L stainless steel. In this publication we report on the research that was done to determine whether non-standard stress corrosion cracked samples can be produced in a controlled way.

Several mechanisms for stress corrosion cracking have been proposed; a useful review of these is given by Jones and Ricker[5]. In the case of chloride cracking of stainless steels, the mechanism must account for the cleavage-like nature of the failure; this has been taken to imply a role of mechanical failure in crack growth[6]. However, the nature of this mechanical role is not clear. In the mechanism of film-induced cleavage[7], corrosion produces a surface product layer which can inject cracks into the underlying metal. Such a surface film was found by transmission electron microscopy of chloride cracks in austenitic stainless steel[8]. In applying this idea, Nishimura[9] proposed that crack growth occurs when the stress at the crack tip reaches a critical value, which is independent of the corrosive environment; the proposed role of the environment is to change the rate at which the local stress at the crack tip increases as a result of corrosion—but there appears not to be direct experimental evidence for the constancy of the fracture stress, and the effect of environment on the rate of stress increase. In contrast with the proposal that the stress corrosion crack grows by brittle failure, it has also been suggested that plasticity is enhanced at the crack tip[10].

The lack of a generally accepted mechanism for chloride cracking of austenitic stainless steels is a difficulty in the present work, because there is no single theoretical framework which can be used to explain the experimental observations.

* *Eskom Holdings (Pty) Ltd., Cleveland, South Africa, Former graduate student-Department of Materials Science and Metallurgical Engineering, University of Pretoria.*

† *Department of Materials Science and Metallurgical Engineering, University of Pretoria, Currently at—Department of Materials Science and Engineering, Carnegie Mellon University, Pittsburgh, USA.*

 SA ISSN 0038–223X/3.00 + 0.00. Paper received Feb. 2009; revised paper received Jul. 2009.

Controlled chloride cracking of austenitic stainless steel tube samples

Experimental approach

Experimental set-up

The experimental set-up consisted of a test rig that was designed to simulate a vessel, pipe or tank that has undergone stress corrosion cracking. A schematic of the test rig is shown in Figure 1. As the figure shows, the sample was a Type 304L stainless steel tube (wall thickness 5 mm), with a hollow Type 310 stainless steel hollow bar at its centre; a heating element was placed in the cavity in the Type 310 bar. Two bar diameters were tested, namely 50 and 75 mm. The Type 310 bar and Type 304L tube sample were linked with two welded-on Type 310 flanges. The outer surface of the Type 304L sample was cooled by exposure to the atmosphere; the temperature difference between the hollow bar and the 304L stainless steel tube induced tensile thermal stress in the 304L tube, superimposed on residual stresses from manufacturing and fabrication. If the flanges were rigid, the expected relationship between the temperature difference between the bar and the sample, ΔT, and the stress, σ, in the tube sample would be as follows:

$$\sigma / E = \alpha \Delta T / \left(1 + A_2 / A_1\right) \quad [1]$$

where E is the elastic modulus, α is the thermal expansion coefficient, A_2 is the cross-sectional area of the tube, and A_1 is the cross-sectional area of the bar. This relationship was tested experimentally.

The residual stresses were measured before and after fabrication of the test rig, as discussed in greater detail elsewhere[11]. Tensile residual stresses were present in the tube before test rig assembly (hoop direction), and compressive residual stresses (longitudinal direction) after welding of the tube into the test rig. Examination of the crack direction after the tests showed that the residual stress direction did not affect the crack direction—the cracks were circumferential, showing that the tensile stress causing cracking was orientated longitudinally (that is, the direction of the thermal stress imposed by heating of the central bar).

The cavity between the tube sample and the central bar was filled with an aqueous solution of 35% $MgCl_2$. The solutions were prepared by dissolving $MgCl_2.6H_2O$ (analytical grade) in demineralized water. The solution was left open to the atmosphere (inside the test rig) to allow for the presence of dissolved oxygen. Evaporation loss was replenished with demineralized water. The solution pH was measured during tests by drawing a sample of the solution from the test rig. The solution sample was allowed to cool to room temperature before measuring its pH. The acidity was maintained at pH=6 by adding dilute hydrochloric acid.

The test rig was instrumented with strain gauges and thermocouples (type J). The electrical circuit with heating element and controller is shown in Figure 2. The controller had an on-off action; the possibility that the resulting stress fluctuations affected crack formation and growth was investigated (as discussed later).

The average sample temperatures during the tests are listed in Table I. As the table indicates, in some of the test rigs it was attempted to increase the stress locally by machining a triangular groove, 0.5 mm wide and 0.5 mm deep, on the inner bore of the sample, at mid-height. The $MgCl_2$ solution temperature was higher than the sample temperature, by 8°C on average.

The three main factors that were expected to influence crack formation and growth rates were sample temperature, stress, and variation in stress (amplitude and frequency). Because the sample was heated by convection and conduction

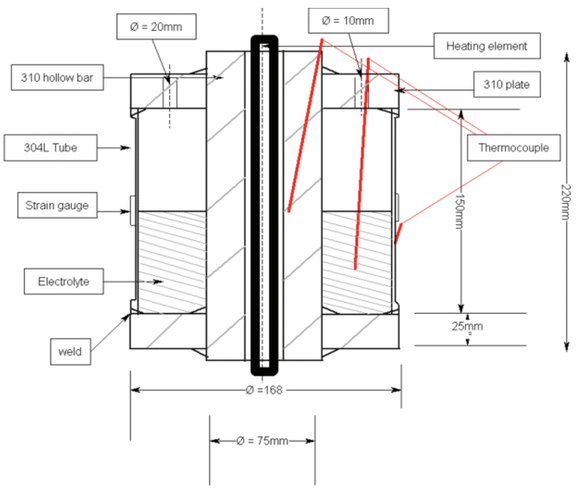

Figure 1—Schematic illustration of test rig

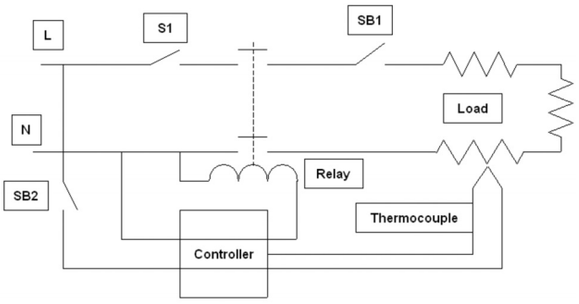

Figure 2—Diagram showing of the electric circuit, including heating elements and temperature controller

Table I

Summary of average sample temperatures during tests

Sample number	Bar diameter (mm)	Average sample temperature (°C)
3A	75	63.5
3B	75	71.0
3C	75	69.3
4A	75	73.0
4B	75	80.9
4C*	75	75.7
4D*	75	77.1
5A	75	83.5
5B*	50	87.2
5C*	50	87.1
6A	75	77.6
7A	75	77.0
8A	50	74.5

*Samples with machined groove on inside surface

from the central bar, and was also stressed by the temperature difference between the sample and the central bar, these factors (temperature, stress and temperature difference) could not be varied independently in the experiments.

Evaluation of cracked samples

During the tests, the samples were examined visually to detect gross defects; seepage solution through the sample wall (resulting in crystallization of white magnesium chloride on the outer surface) indicated the presence of a through-wall crack; a sample was removed from the test as soon as such a crack was detected. The flanges were cut off and the samples were sectioned longitudinally to allow examination of the interior surface. The crack morphology was identified and crack distribution was determined by counting cracks on the internal surface of the tube using optical and stereo microscopes. Crack depth measurements and fracture surface analysis were done with a scanning electron microscope.

The surface cracks counted were mapped for every sample. An estimate of the average crack formation rate was obtained by dividing the crack density by the exposure time. Cracks which intersected were counted as separate entities. The minimum length of cracks which were counted was 0.82 mm (for stereo microscopy of internal surface cracks), and for optical microscopy of polished cross-sections the minimum measured crack depth (at 500X magnification) was 20 μm.

Results and discussion

Measured strain and temperature

Typical test results of temperature and strain are shown in Figures 3 and 4. The temperatures measured in the central bar, in the solution and on the outside surface of the sample (see Figure 1 for the thermocouple locations) are shown in Figure 3. The temperature difference between the bar and the sample followed an inverse sawtooth pattern, of rapid increases followed by slower decreases; the strain in the sample followed the same pattern (Figure 4). The sawtooth pattern was due to the heating element being turned on and off by the controller in order to maintain test temperature. The frequencies of the fluctuations are given in Table II.

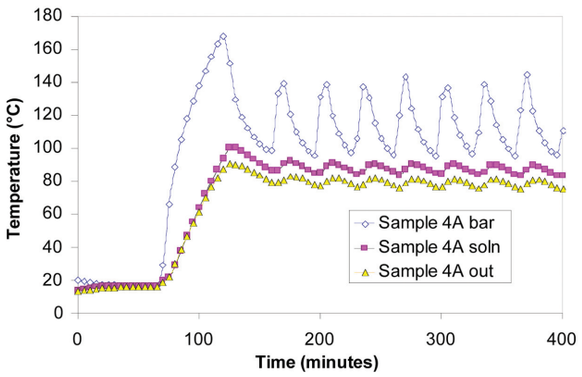

Figure 3—Typical temperature variation with time inside the test rig, at the three thermocouple positions as shown in Figure 1. The results are for sample 4A, at the start of the test

As shown by Equation [1], the tensile stress in the sample is expected to be proportional to the temperature difference between the bar and the sample. This predicted relationship is tested in Figure 5, which reveals that the measured strains are approximately half the predicted values. This is because coupling between the bar and the sample was not completely rigid (as assumed in the simple analytical model); flexure of the flange which coupled the bar to the sample allowed for some relief of the thermal stress. Finite-element calculations (reported in detail elsewhere[11]) confirmed this effect.

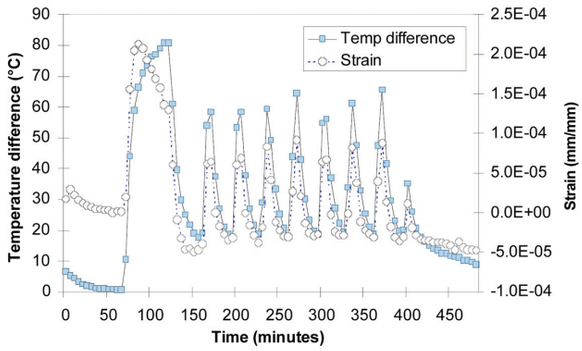

Figure 4—Correspondence between the temperature difference between the central bar and the tube sample, and the measured strain in the tube sample; data shown are for sample 4A, for the same period as the data of Figure 3

Table II

Frequency of stress fluctuations during tests

Test	Frequency of stress fluctuations (Hz)
Test 3	$4.2X10^{-4}$
Test 4	$4.2X10^{-4}$
Test 5	$7.5X10^{-4}$

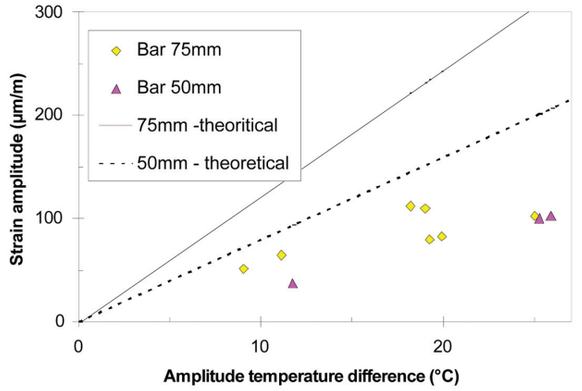

Figure 5—Difference between the predicted relationship between elastic strain in the tube and the bar-tube temperature difference (lines) and the observed relationships (data points). Each data point is the average for the entire test period

Effect of varying stress on failure

The results could be used to test whether cyclic loading contributes significantly to crack growth. It was possible to perform this check because the amplitude of the strain cycles varied somewhat during the tests, and with different average sample temperatures. If cyclic loading played an important role, one would expect a significant contribution of the cyclic strain (hence the cyclic thermal stress) on the rate of crack growth and, hence on the time to failure[12]. However, the results summarized in Figure 6 show that, while there was some variation in the cyclic strains in different tests, there is no correlation between the cyclic strain and the time to failure. Rather, the time to failure correlates with the sample temperature and less strongly with the applied (average) stress; this behaviour is to be expected of chloride cracking rather than corrosion fatigue.

The absence of an effect of stress cycling does agree with the arguments advanced by Pugh,[6] who suggested that stress corrosion cracks advance discontinuously, with each advance a brittle failure. Experimental evidence for such discontinuous advance has been summarized by Sieradzki and Newman.[7] If one assumes that the distance by which the crack advances per event is 0.5 μm, as for 310 stainless steel in boiling magnesium chloride solution,[6] and taking the typical crack growth rate in this work to be 6 μm/hour (see Figure 7 later in this paper), then the time between crack growth events is estimated to be 300 s. This is significantly shorter than the period of the temperature and stress fluctuations, of which the period was around 2500 s (Table II). In this view, in this work the stress fluctuations simply occurred at too low a frequency to influence crack growth significantly. The low crack velocity, corresponding to stress intensities just above $K_{I\,SCC}$, with crack velocities much lower than the plateau values, supports a direct role of mechanical deformation in crack growth.[13] This is also in line with a crude estimate of the stress intensity in these tests: for the typical average stress of 100 MPa (Figure 6), and taking a crack length of 5 mm (sample wall thickness), the stress intensity (calculated as $\sigma[\pi a]^{0.5}$) is estimated as 12.5 MPa.m$^{0.5}$, similar to the reported threshold stress intensity for Type 316 in hot magnesium chloride solutions.[13]

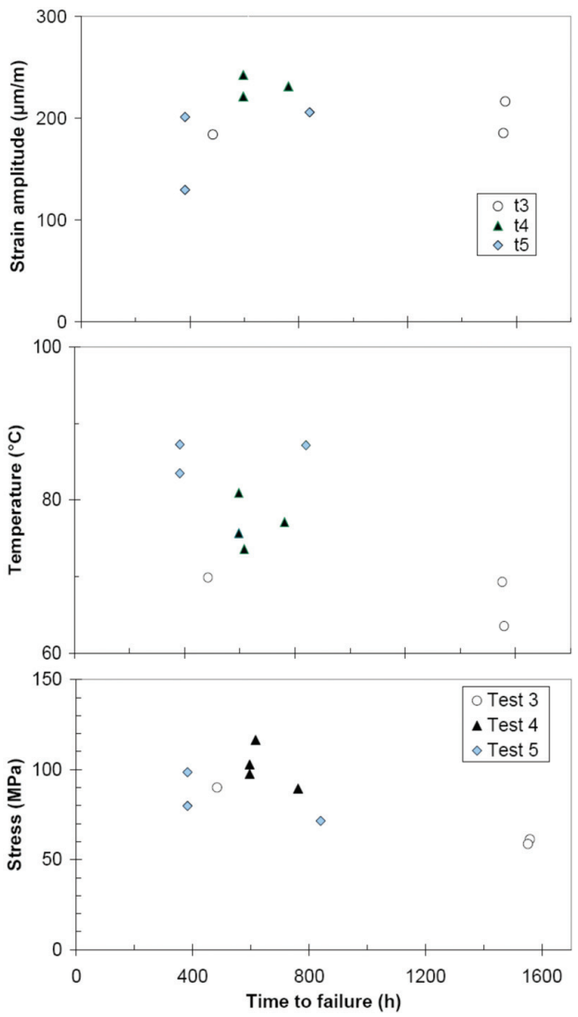

Figure 6—Relationship between time to failure (first through-thickness crack) and strain amplitude, sample temperature, and average stress

Visual examination and metallography

The test rigs were visually inspected for leaks. Through-thickness cracks were recognized by white magnesium chloride deposit that crystallize on the outer surface of the tube sample. The first visible crack leak was the definition of failure, at which time the test was stopped for that particular sample.

The internal surfaces were discoloured at the end of the tests because of the presence of corrosion products. In the case of samples 3A and 3C the internal surface was greenish, probably due to the release of chromium through pitting

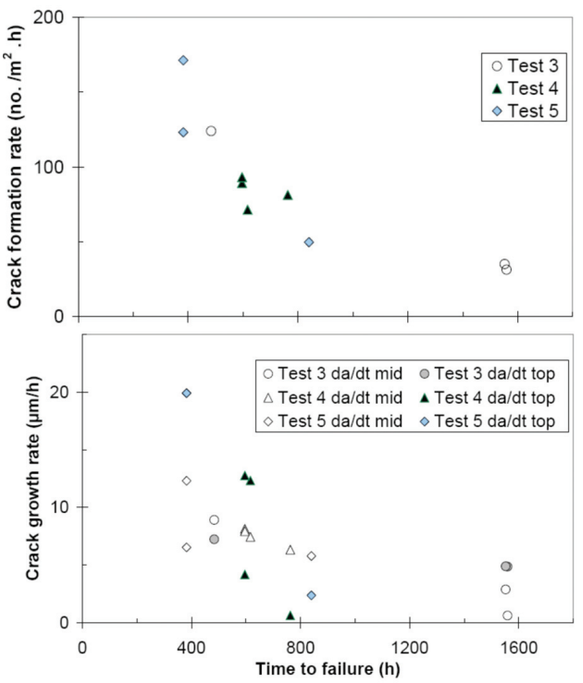

Figure 7—Average rate of formation of cracks (upper figure) and average growth rates of the cracks (lower figure) for the three main sets of tests

corrosion; the internal surfaces of other samples were reddish-black. Many cracks were visible on the internal surfaces of all samples, above and below the water line. The majority of cracks did not pass through the wall thickness, a result of the experimental approach to stop the test as soon as a sample displayed a through-thickness crack. Some cracks were also observed on the central bar and the end flanges. In some of the samples pits were associated with cracks. However, because of the possibility of corrosion after crack growth started, it is not possible to state that the cracks initiated from corrosion pits.

The surface cracks counted were mapped for every sample. Samples that took longer to fail generally had lower average crack formation rates (Figure 7).

The distribution of crack depths was measured on cross-sections through the samples, by optical microscopy. It is recognized that this can underestimate crack depth, if the crack tip does not fall within the polishing plane, but this method does give a way of comparing different samples. An average crack growth rate was calculated, assuming that the deepest cracks grew for the entire exposure period; the results are presented in Figure 7. Because the sample wall thickness was larger close to the sample top than at the midpoint (see Figure 1), the growth rate is not simply inversely proportional to the time to failure—in some cases the longest crack (close to the sample top) was not the crack which led to leaking.

A typical distribution of crack depths is shown in Figure 8. The flat nature of the distribution—with many shallow cracks as well as deep cracks—indicates that cracks nucleated throughout the test period.

The high crack density and wide distribution of crack depths illustrate that the approach used in this work cannot be used to produce samples with just a few, well-defined cracks. The aim of this project was to produce cracked samples which can serve as test pieces for a laser-welding repair method. Whether these samples are appropriate for testing the repair method depends on the actual in-service stress corrosion cracked components having similarly high crack densities. Evaluation of in-service components did not form part of the scope of the work reported here.

The distribution of crack densities on the sample surfaces followed essentially two patterns, see Figure 9. In the cases where the electrolyte level was maintained at half the height of the tube sample (runs 4C and 4D) the crack density peaked around the water line, presumably because of locally increased salt concentration just above the water line, through splashing and evaporation, or 'creeping' of the salt[14]. For samples which were kept filled during the runs, the crack density peaked at the upper and lower ends of the samples, which is where the temperature was highest; the predicted temperature distribution along the sample height (based on finite element calculations) is also shown in Figure 9. Based on the appearance of the sample cross-sections, the machined notches did enhance crack formation locally (Figure 10), but there was no noticeable effect on the time to failure.

Examination of polished and etched cross-sections confirmed that the cracks were transgranular and branched, as expected of chloride cracking of unsensitized austenitic stainless steel[2]; see Figure 11. It was difficult to study the fracture surface, because it had been corroded, and also because of the presence of nonconductive material (electrolyte residues or corrosion products) on the fracture surface. However, areas which could be examined confirmed the expected quasi-cleavage appearance of chloride cracking—see Figure 11.

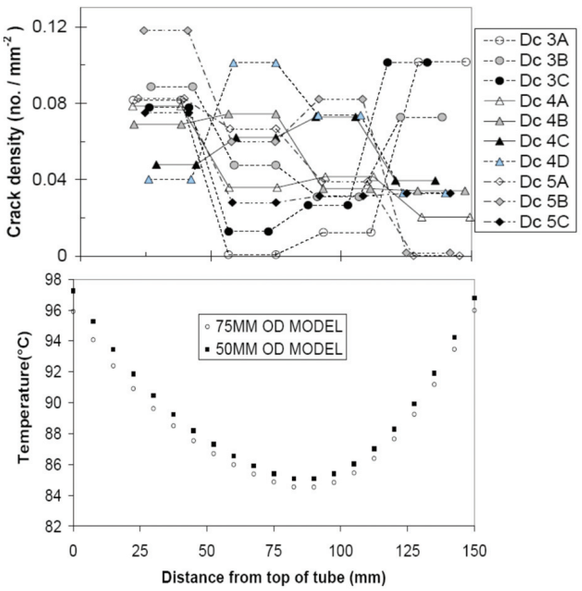

Figure 9—Variation of crack density with height on the interior surfaces of the sample (upper figure), and the variation in sample temperature with height as predicted by the finite element calculations (lower figure)

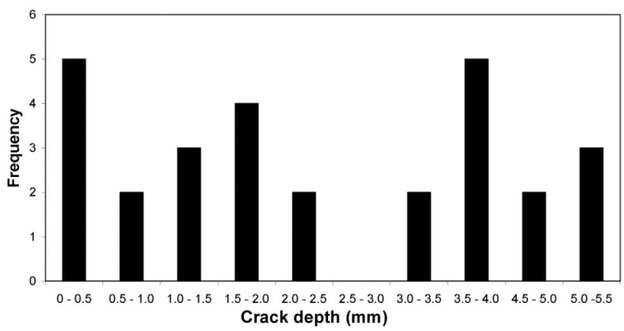

Figure 8—Distribution of crack depths, as measured on polished cross-section; example shown is for sample 4D at mid-height

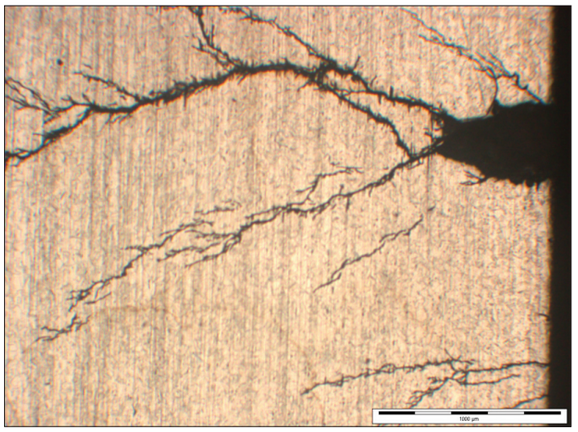

Figure 10—Crack nucleation from a machined notch (located in the upper right-hand part of the image), as seen on a sample cross-section (optical micrograph; micron marker 1 mm long)

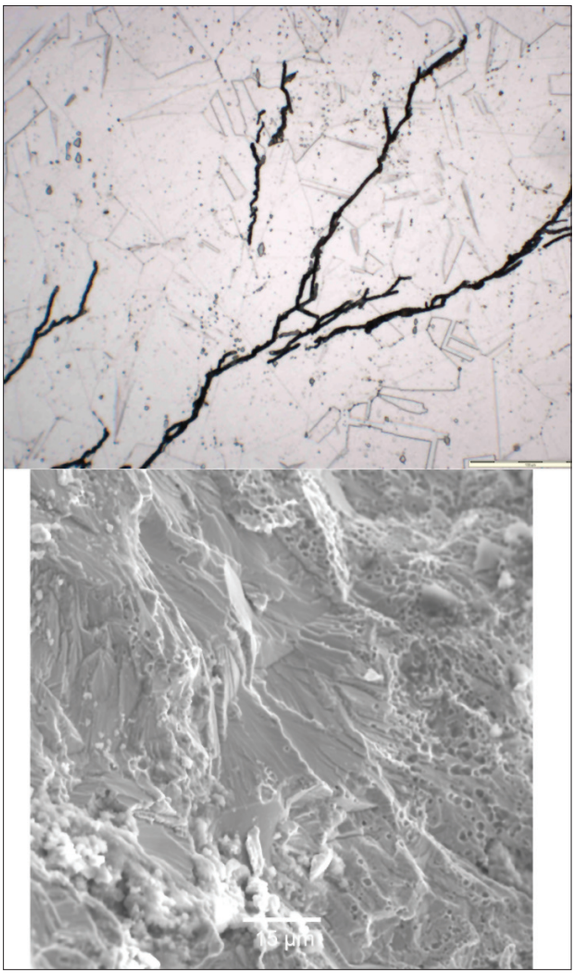

Figure 11—Appearance of cracks. Upper figure: optical micrograph of polished and etched cross-section (scale marker is 100 µm long). Lower figure: Scanning electron micrograph of a fracture surface (sample from test 4A) illustrating the quasi-cleavage nature of crack growth

Conclusion

In the test rig constructed in this project, thermal stress—caused by the difference in temperature between the bar and the tube (sample)—caused transgranular cracking of the sample. Low-frequency cyclic loading did not appear to affect cracking significantly. The experimental method resulted in the formation of multiple branched cracks in the samples.

Acknowledgements

We are grateful for the financial support provided by the Corrosion Institute of Southern Africa, Eskom Holdings Limited, and the University of Pretoria (UP), and to staff of the latter two institutions for technical assistance. In particular, Mark Newby and his team are thanked for assistance with strain gauge work, Ronny Scheepers for finite element modelling, and Dr Thobeka Pete for technical editing.

Reference

1. Sedriks, A.J. *Corrosion of stainless steels*, 2nd edition. John Wiley & Sons, 1996.
2. Kowaka, M. *Metal corrosion damage and protection technology*, (Chapter 6: Stress corrosion cracking of stainless steels), Allerton Press (1990). pp. 347–467.
3. Tverberg, J.C. Stainless in the Brewery. *Technical Quarterly of the Master Brewers Association of the Americas*, vol. 38, no. 2, 2001. pp. 67–82.
4. Laser welding, CSIR, www.csir.co.za accessed on 30 January 2006.
5. Jones, R.H. and Ricker, R.E. Mechanisms of stress-corrosion cracking. *Stress-corrosion cracking*, R.H. Jones (ed.). ASM 1992.
6. Pugh, E.N. Progress toward understanding the stress corrosion problem. *Corrosion*, vol. 41, 1985. pp. 517–526.
7. Sieradzki K. and Newman, R.C. Brittle behaviour of ductile metals during stress-corrosion cracking. *Philosophical Magazine A*, vol. 51, 1985. pp. 95–132.
8. Nisbet, W.J., Lorimer, G.W., and Newman, R.C. A transmission electron microscopy study of stress corrosion cracking in stainless steels. *Corrosion Science*, vol. 35, 1993, pp. 457–469.
9. Nishimura, R. Characterization and perspective of stress corrosion cracking of austenitic stainless steels (type 304 and type 316) in acid solutions using constant load method. *Corrosion Science*, vol. 49, 2007. pp. 81–91.
10. Magnin, T., Chambreuil, A., and Chateau, J.P. Stress corrosion mechanisms in ductile FCC materials. *International Journal of Fracture*, vol. 79, 1996. pp. 147–163.
11. Raseroka, M.S. Controlled chloride cracking of austenitic stainless steel. MSc dissertation, University of Pretoria, 2008.
12. Hertzberg, R.W. *Deformation and fracture mechanics of engineering materials*, second edition. Wiley, 1983. pp. 570–581.
13. Russell, A.J. and Tromans, D. A fracture mechanics study of stress corrosion cracking of Type-316 stainless steel. *Metallurgical Transactions A*, vol. 10A, 1979. pp. 1229–1238.
14. Washburn, E.R. The creeping of solutions. *Journal of physical chemistry*, vol. 31, 1927. pp. 1246–1248. ◆